THE JOURNAL OF PHYSICAL CHEMISTRY Letters

Cite This: J. Phys. Chem. Lett. 2018, 9, 6412−6420

Letter

pubs.acs.org/JPCL

Unraveling the Oxidation and Spin State of Mn−Corrole through X-ray Spectroscopy and Quantum Chemical Analysis

Mateusz Paszkiewicz,[†] Timur Biktagirov,[‡] Hazem Aldahhak,[‡] Francesco Allegretti,[†] Eva Rauls,[§] Wolfgang Schöfberger,[⊥] Wolf Gero Schmidt,[‡] Johannes V. Barth,[†] Uwe Gerstmann,*[,‡] and Florian Klappenberger*[,†]

[†]Physics Department E20, Technical University of Munich, James-Franck-Strasse 1, 85748 Garching, Germany

[‡]Department of Physics, Paderborn University, Warburger Strasse 100, 33098 Paderborn, Germany

[§]Institutt for Matematikk og Fysikk, University of Stavanger, 4036 Stavanger, Norway

[⊥]Institute of Organic Chemistry, Johannes Kepler University, Altenberger Straße 69, 4040 Linz, Austria

Supporting Information

ABSTRACT: The interplay between Mn ions and corrole ligands gives rise to complex scenarios regarding the metal centers' electronic properties expressing a range of high oxidation states and spin configurations. The resulting potential of Mn−corroles for applications such as catalysts or fuel cells has recently been demonstrated. However, despite being crucial for their functionality, the electronic structure of Mn−corroles is often hardly accessible with traditional techniques and thus is still under debate, especially under interfacial conditions. Here, we unravel the electronic ground state of the prototypical Mn-5,10,15-tris(pentafluorophenyl)corrole complex through X-ray spectroscopic investigations of ultrapure thin films and quantum chemical analysis. The theory-based interpretation of Mn photoemission and absorption fine structure spectra (3s and 2p and $L_{2,3}$-edge, respectively) evidence a Mn(III) oxidation state with an $S = 2$ high-spin configuration. By referencing density functional theory calculations with the experiments, we lay the basis for extending our approach to the characterization of complex interfaces.

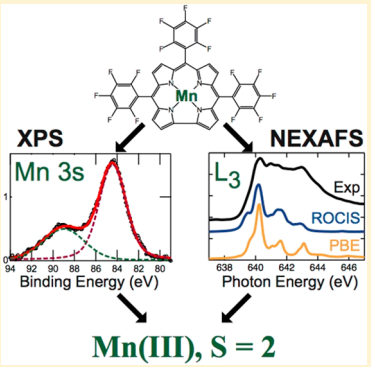

Tetrapyrrole metal complexes are an important class of compounds that have been increasingly studied in recent years due to their promise for applications in catalysis, sensors, and solar cells.[1−3] Within this class, the corrole macrocycle (Cor) expresses the intriguing property of stabilizing incorporated metal centers in high oxidation states.[4,5] Such complexes play an important role in catalytic reactions by enabling favorable pathways via intermediates or as oxygen or carbon carriers.[6] The energetics of these intermediates as well as their electronic configurations are crucial for such applications. Manganese is a transition metal (TM) capable of adopting a wide range of oxidation states, rendering it highly suited for catalytic conversion,[7,8] molecular magnets,[9,10] and coordination frameworks for gas separation[11] and asymmetric synthesis.[12] The potential of Mn-containing complexes has been equally appreciated in interfacial systems.[13−18] Combining these effects, Mn−corroles express nontrivial physicochemical behavior related to their specific electronic properties such as their oxidation state and spin configuration.[19−22] For example, Mn−Cor($OPPh_3$)[23] and Mn−Et_2Me_6Cor[24] have been characterized in the solid state as Mn(III) high-spin complexes, in contrast to Cu−Cor[25] or Zn−$Cl_2Mesityl_3$Cor,[26] which exist as TM(II)$Cor^{2-,*}$ radical species. Mn−Et_2Me_6Cor, on the other hand, exhibits a temperature-dependent electronic ground-state configuration in the presence of nitrogenous bases in the solvent. Instead of adopting a high-spin configuration, $S = 2$, Mn−corroles tend to undergo a transition to an intermediate-spin state by electron transfer from the corrole ligand to the metal ion. As a result of this intramolecular transfer, the manganese ion is reduced to Mn(II), whereas the corrole forms a radical cation ($Cor^{2-,*}$).[24] Due to this phenomenon involving the physical oxidation state of the incorporated metal center and the capability of the macrocycle to exist as a radical, the corrole family has been assigned to the group of noninnocent ligand species.[27] Recent studies of H_2−$Cl_2Mesityl_3$Cor in the solid state[26] as well as H_3−$(F_5Ph)_3$Cor on a Ag(111) surface[28] indeed revealed the high stability of such radical species.

In view of its importance, it is unfortunate that the analysis of the electronic ground state of Mn−corrole derivatives is complicated by their tendency to be "silent"[29] in conventional electron paramagnetic resonance (EPR) due to large zero-field splitting in integer spin systems. Highly demanding high-frequency EPR is required to probe the electronic ground state for such complexes.[23] Similarly, the analysis of nuclear magnetic resonance (NMR) spectra can be challenging, as exemplified by the case of Mn(III) porphyrins.[30,31] As a consequence, alternative methods to identify the electronic

Received: August 16, 2018
Accepted: October 2, 2018
Published: October 17, 2018

DOI: 10.1021/acs.jpclett.8b02525
J. Phys. Chem. Lett. 2018, 9, 6412−6420

structure are highly desirable to achieve the required understanding of Mn−corroles and metal−corroles in general.

Here, we present the first X-ray spectroscopy characterization of the prototypical Mn-5,10,15-tris(pentafluorophenyl)corrole (Mn−$(F_5Ph)_3$Cor; see also Scheme 1)

Scheme 1. Chemical Structure of Mn-5,10,15-tris(pentafluorophenyl)corrole (Mn−$(F_5Ph)_3$Cor)[a]

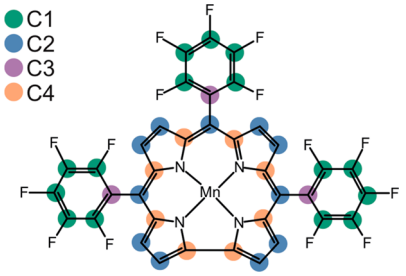

[a]Following refs 32 and 33, the carbon atoms are divided into four groups of quasi-equivalent species; their given ratio (15:11:3:8) is used as a starting point for XPS analysis (cf. Figure 1a).

supported by quantum chemical and density functional theory (DFT) calculations in order to characterize the oxidation state as well as ground-state spin configuration of the central Mn ions. A state-of-the-art combination of theoretical analysis tools allows us to interpret the multiplet splitting in the Mn 3s core-level data monitored by X-ray photoelectron spectroscopy (XPS) and the shape of near-edge X-ray absorption fine structure (NEXAFS) spectra of the Mn L_3-edge. We demonstrate that the complex contains a Mn(III) center in the high-spin (S = 2) ground-state configuration. Importantly, our work also provides a reference for the DFT-based treatment of periodic Mn complexes in the solid state, rendering our approach suited for application to interfaces including the theoretically challenging corrole−metal substrate case.

In the first step, an "ultrapure" multilayer film of Mn−$(F_5Ph)_3$Cor was prepared by starting from a highly pure molecular powder and then utilizing organic molecular beam epitaxy (OMBE) under ultrahigh vacuum (UHV) conditions to evaporate the corrole molecules onto an atomically clean Ag(111) surface (see also the Methods section, Sample Preparation). The combination of these methods achieves thin films significantly cleaner than standard evaporation techniques such as drop-casting or chemical vapor deposition. The quality and the chemical integrity of the prepared film were investigated by recording XPS signatures. The C 1s signal (Figure 1a) can be fitted with four components similarly to its free base equivalent.[32,33] The experimentally determined area ratios for the individual components (15:9:3:7) nicely match the theoretical stoichiometric composition (15:11:3:8) of the synthesized species. The N 1s spectrum (Figure 1b) consists of a single peak with a binding energy of 398.9 eV, which is characteristic for metalated corroles, porphyrins, and phthalocyanine complexes.[34−36] The F 1s region (Figure 1c) exhibits a single feature with a binding energy (688.3 eV) comparable to that of H_3−corrole.[32] Therefore, the collected C 1s, N 1s, and F 1s XP spectra evidence the high purity of the adsorbed layer and the integrity of the individual molecules within the latter, confirming the quality of the condensed film.

To assess the properties of the incorporated metal centers, we measured the Mn 2p and Mn 3s XPS signatures, which are presented in Figure 1d−f. For the interpretation of their line shapes, a number of aspects should be considered.

First, due to the spin−orbit (SO) splitting, the features of the 2p region are separated into two subregions. Specifically, the $2p_{3/2}$ region appears in the energy range from 640 to 650 eV, and the $2p_{1/2}$ region is positioned between 650 and 660 eV. Their intensity ratio of 2:1 follows exactly that of their total

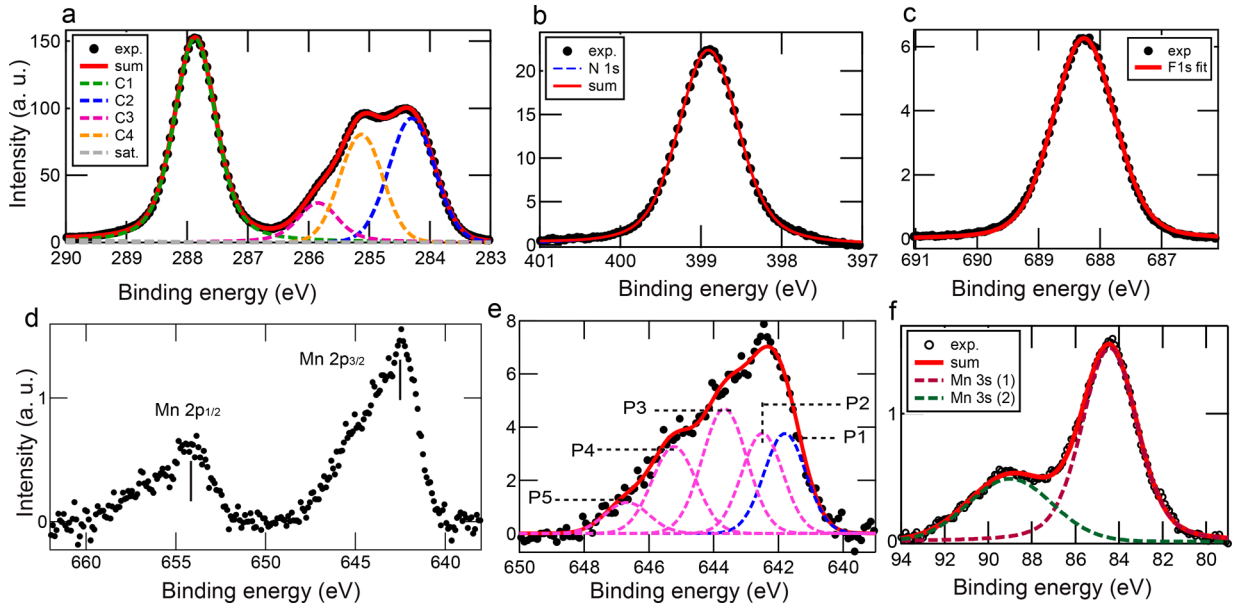

Figure 1. XPS data of an ultrapure Mn−$(F_5Ph)_3$Cor thin multilayer film on a Ag(111) surface. (a) C 1s, (b) N 1s, and (c) F 1s spectra with the corresponding fit analysis, whereby in (a) four different groups of quasi-equivalent carbon atoms with an intensity ratio of 15:9:3:7 have been taken into account (cf. Scheme 1 and refs 32 and 33). (d) The high-resolution Mn 2p region consists of two sets of peaks due to spin−orbit splitting. The black bars mark the maxima utilized to obtain the splitting value. (e) Fit of the Mn $2p_{3/2}$ region. (f) Mn 3s spectrum and fit with two exchange-split components ^{6}D and ^{4}D, labeled "Mn 3s (1)" and "Mn 3s (2)", respectively.

DOI: 10.1021/acs.jpclett.8b02525
J. Phys. Chem. Lett. 2018, 9, 6412−6420

spin multiplicities $2j + 1$ (4:2). The multiplet splitting also strongly affects their line shape, generating a tail on the higher binding energy side of both regions. Detailed analysis of the resulting complex line shape of the Mn $2p_{3/2}$ spectra can be performed using the multiplet structure parameters of free 3d TM ions determined by Gupta and Sen.[37−39] In the literature, these quantities have been used for the successful interpretation of Mn $2p_{3/2}$ signatures for a variety of systems such as MnOOH, MnO_x, and organometallic complexes like Cl−MnTPP or Mn(III) ferrocenyl-β-diketonato complexes.[14,23,40] To assign the oxidation state of the Mn ion, we compare with the Gupta−Sen coefficients expected for II, III, and IV oxidation states.[39] We used the multiplet parameters, i.e., relative peak shifts and intensity ratios, of free Mn ions[39] as initial values for the fitting procedure. The result of the latter is presented in Figure 1e, while the final values of the coefficients are listed in Table 1. The Mn(II) state can be ruled out due to very poor matching in both, the relative binding energies ΔE_B (in particular P5), as well as in the relative intensities of the individual components. Conversely, both the Mn(III) and the Mn(IV) states express values for ΔE_B compatible with the experiment; however, only for the III case are the relative intensities also in good agreement with the experimental observation, while the IV case clearly deviates. Overall, the line shape of the XPS $2p_{3/2}$ signature supports the conclusion of a III oxidation state of the Mn ion in the Mn−$(F_5Ph)_3$Cor complex. Some degree of remaining discrepancy can be explained by the existence of shake-up or shake-off satellites in this energy range because the theoretical analysis used does not consider such multielectron processes and other subtle final state effects. Moreover, the exact strength of ligand/crystal field can have crucial impact on the exact intensity ratio redistribution over diverse eigenstates and affect the overall line shape of the spectrum.[38]

Table 1. Relative Binding Energies (ΔE_B), FWHMs, and Intensity Ratios of the Individual Components of the Mn $2p_{3/2}$ Core-Level Line (cf. Figure 1e) in Comparison to Theoretical Values from Nesbitt[39] for Free Mn Ions of the Given Oxidation States[a]

	ΔE_B (eV)				rel. intensity (%)			
	exp	theory (Gupta−Sen)			exp	theory (Gupta−Sen)		
peak		II	III	IV		II	III	IV
P2	0.7	1.3	0.7	1	100	75	100	67
P3	1.9	2.4	1.6	1.9	132	51	135	33
P4	3.4	3.1	2.4	2.9	90	25	70	14
P5	4.9	7.6	4.2	4.9	32	15	30	23

[a]Values (intensities and energies) are given relative to those of the P1 peak; the experimental binding energy of peak P1 is 641.8 eV.

In similar systems, the SO splitting of the 2p core level into distinct $2p_{3/2}$ and $2p_{1/2}$ components has been shown to be sensitive to the electronegativity of the involved side groups:[32] upon modification of Mn(III) β-diketonato ligands, different values are observed in the range of 11.58−11.96 eV. Here, we observe a splitting of 11.6 eV between the two black lines marking the selected maxima (Figure 1d). Applying DFT relativistically, i.e., by numerically solving Dirac's equation for the free atom, we calculated average SO splittings of 11.06 (± 0.01) eV irrespective of the oxidation state and the total spin S (see also the SI, Table S1). This renders the SO splitting of the Mn 2p levels sensitive to the attached ligands but, unfortunately, not distinctive of either the specific spin or, in particular, the oxidation state of the Mn ion.

More valuable information can be gained from the Mn 3s XPS spectrum, presented in Figure 1f, which has a less complex line shape than its 2p counterpart but also exhibits a characteristic splitting in the final state due to the exchange coupling of the remaining (spin-up or -down) 3s electron to the 3d shell. The spectrum consists of two peaks, whereby the first one exhibits a binding energy of 84.3 eV. This state corresponds to a $^{2S+2}$D final state representing a $3s\uparrow 3d^n$ high-spin ($S' = S + 1/2$) configuration. The second peak is located at 89.1 eV and represents the ^{2S}D state, where *after photoelectron emission* the remaining electron in the 3s orbital has spin-down character yielding a $3s\downarrow 3d^n$, i.e. $S' = S - 1/2$ configuration. The energy difference between these two $^{2S'+1}$D spin states is 4.8 eV (cf. Figure 1f). In bulk materials, e.g., Mn_xO_y manganese oxides, this splitting is diagnostic of the oxidation state,[41,42] whereby a value of 4.8 eV is borderline between III and IV oxidation states. Due to the generally lower photoionization cross section of the Mn 3s orbital in comparison to the Mn 2p orbitals and due to the small amount of Mn atoms in a thin film of corrole complexes, this signal is rarely used for the analysis of complexed atoms. However, Fujiwara et al. showed that also for molecular systems the XPS 3s signature can be much more strongly affected by the oxidation state of the ligated atom than the 2p orbital.[43]

Table 2. $^{2S+2}$D−^{2S}D Multiplet Splitting of Mn 3s XPS Calculated for Various Oxidation and Spin States[a]

		charged free atom	*neutral* molecule			*neutral* molecular crystal	
oxidation state	spin state S	B3LYP (AE)	B3LYP (AE)	PBE+U (PW)	PBE (PW)	PBE+U (PW)	PBE (PW)
Mn(II)	5/2	6.25 (1.25)					
	3/2	3.82 (1.27)					
	1/2	1.27 (1.27)					
Mn(III)	2	5.44 (1.36)	4.74	4.60	4.20	4.54	4.18
	1	2.76 (1.38)	2.60	2.40	2.45	2.46	2.51
Mn(IV)	3/2	4.41 (1.47)					
	1/2	1.47 (1.47)					

[a]Differences of the ionization energies of the 3s spin-up/down electrons are in eV. The results of the free Mn ion reference (charge state = oxidation state) and the *neutral* Mn−$(F_5Ph)_3$Cor molecule were obtained from AE (B3LYP) finite size DFT calculations. For the molecule and for a molecular crystal, tentatively adapted from the solid state of the free-base species (see also ref 32 and Figure S4), values derived from pseudopotential PW-based supercell calculations (PBE, PBE+U) are also given. For the free ion, the spin-multiplet splitting per unpaired electron (total value divided by $2S$) is also given in parentheses.

DOI: 10.1021/acs.jpclett.8b02525
J. Phys. Chem. Lett. 2018, 9, 6412−6420

Table 3. Total Energy Differences (in eV per Mn ion) for Different Spin States (with Respect to the $S = 2$ Ground State) of the Neutral Mn−$(F_5Ph)_3$Cor Molecule and for a Molecular Crystal (cf. Figure S4), Obtained Using Different XC Functionals, All Providing Mn(III) Ground States

		free ion	molecule		molecular crystal	
	total spin S	B3LYP (AE)	PBE+U (PW)	PBE (PW)	PBE+U (PW)	PBE (PW)
Mn(III)	2	0.00	0.00	0.00	0.00	0.00
Mn(III)	1	+ 1.02	+ 0.71	+ 1.05	+ 1.05	+ 1.36
Mn(III)	0	+ 1.38	+ 1.06	+ 1.40	+ 1.45	+ 1.76

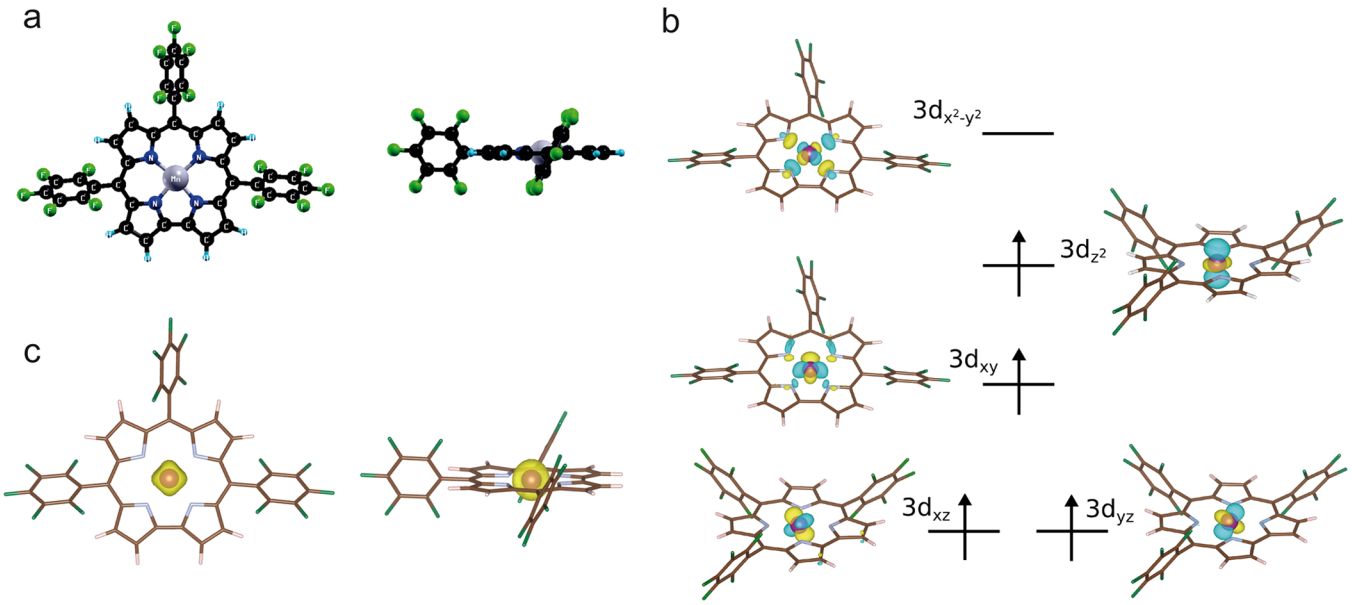

Figure 2. (a) DFT-optimized structure of Mn−$(F_5Ph)_3$Cor (shown for the PBE functional). (b) Schematic MO diagram including illustration of the spin distribution in the corresponding 3d orbitals. (c) For comparison, the total spin density (depicted in top and side views) is also shown.

In order to elucidate the impact of the formal oxidation and spin states on the Mn 3s XP spectrum of the molecule species, the multiplet splitting values of Mn−$(F_5Ph)_3$Cor have been obtained by two DFT approaches employing all-electron (AE) and pseudopotential plane-wave (PW) calculations, respectively (for details, see the Methods section, DFT Calculations). PW modeling of the spin states of the molecule was performed within a supercell approach (Quantum ESPRESSO package[44]) in connection with PBE[45] and PBE+U functionals.[46,47] The combination of a PW supercell and AE finite size modeling is chosen due to the fact that the supercell approach allows for proper treatment of periodic structures, e.g., the molecular species in the solid state (see also Figure S4). It can be easily extended toward the monolayer regime but initially requires careful evaluation of the electron−hole interaction benchmarked here with the AE modeling (see also the Methods section). The basically identical *energetic* results (see Tables 2 and 3) obtained for the isolated molecules and the molecular crystal show that within a Mn−$(F_5Ph)_3$Cor multilayer the Mn centers experience only minor effects of intermolecular interactions, justifying to a certain extent finite-size treatment of single molecules as a reference for the multilayer regime, which has been done with an AE approach (ROCIS,[48] ORCA code[49]) using the B3LYP hybrid functional.[50−52]

The atomic data for the Mn 3s core level presented in Table 2 indicate a minor dependence of the Mn 3s multiplet splitting on the *oxidation* state. The by far strongest effect is observed when changing the spin state: About 1.27, 1.37, and 1.47 eV per unpaired electron (total values divided by 2S) are contributed to the splitting in the II, III, and IV oxidation states, respectively, rendering the Mn 3s multiplet splitting, in particular, diagnostic for the *spin* state. For Mn ions in a molecular environment, the multiplet splittings become slightly smaller. A total value (B3LYP) of 4.74 eV for the Mn(III) state of the isolated molecule suggests a high-spin ($S = 2$) state and fits nearly perfectly to the experimental value.

Indications for the Mn(III), $S = 2$ ground state are further supported by the calculated total energies of the distinct configurations: Table 3 lists relative energies for electronically and structurally relaxed Mn−$(F_5Ph)_3$Cor structures exhibiting different spin states. The results were referenced against the energy of the high-spin state ($S = 2$). Independent of the exchange−correlation (XC) functional as well as of the method of modeling (isolated molecules or molecular crystal), all calculations support the same tendency of the energetic order and clearly favor the high-spin state. The intermediate-spin state ($S = 1$) is more than 0.7 eV higher in energy, and thus, its occupation probability appears to be negligible at room temperature and even far above. Notably, the formal II and IV oxidation states are also not easily addressable by recharging the molecule because the HOMO and LUMO are mainly due to the side-group carbon orbitals, (see also Figure S1); adding/removing electrons from the entire system changes the occupation of C orbitals predominantly, demonstrating that the Mn 3d shell does not participate in an oxidation process.

The favored structure of the Mn(III)−$(F_5Ph)_3$Cor $S = 2$ ground state does not depend considerably on the XC

DOI: 10.1021/acs.jpclett.8b02525
J. Phys. Chem. Lett. 2018, 9, 6412−6420

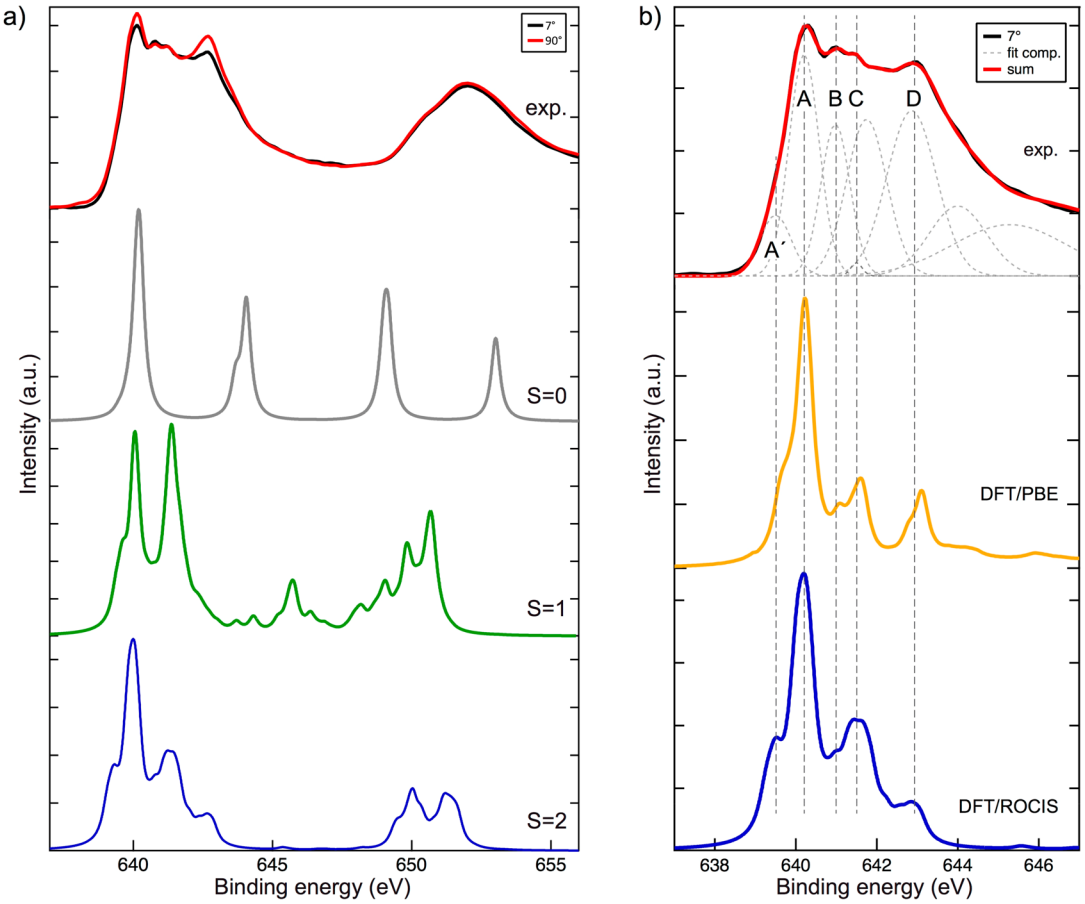

Figure 3. (a) High-resolution experimental Mn $L_{2,3}$-edge of a Mn−$(F_5Ph)_3$Cor thin film on a Ag(111) surface (top panel) measured with two different incidence angles of 7° (black curve) and 90° (red curve) and theoretical Mn $L_{2,3}$-edges calculated with the DFT/ROCIS method (ORCA) for S = 0, 1, and 2 (lower panels). (b) Comparison of the experimental L_3-edge (top) with the mixed (30% core hole) DFT/PBE (middle) and DFT/ROCIS method (bottom) for S = 2.

functional; even in the relaxed molecular crystal, the individual molecules largely retain their conformational properties (see also Figure S4). The geometric structure of an isolated species as obtained for the PBE functional is depicted in Figure 2a. The macrocycle is almost planar, and the phenyl rings are rotated in a similar fashion as those for the free base analogue.[32] The Mn ion is located in the plane of the macrocycle, in line with experimental findings for related, nonaxially ligated Mn−corrole complexes.[53] The average Mn−N bond length of 1.901 Å closely resembles crystallographic data (1.894 Å) obtained for Me_2Et_6Mn−Cor in its crystal structure.[54] The calculated projected density of states (PDOS) of the Mn 3d orbitals provide further insight into the electronic properties of the incorporated Mn ion (see also Figure S1). The energetic positioning as well as the occupation of the individual 3d orbitals are summed up in Figure 2b; the 3d orbital energies can be found in the SI (Table S2). All calculations indicate that the degenerate d_{xz} and d_{yz} orbitals have the lowest energies. Although the exact values depend on the XC functional used, the d_{xy} and d_{z^2} orbitals are about 0.3 and 0.8 eV higher in energy, respectively. The $d_{x^2-y^2}$ orbital is positioned 4 eV higher in energy, hence more than 3 eV above the carbon-originating HOMO orbitals (see also Figure S1). Together with the tendency to high-spin states, it is this separation of the $d_{x^2-y^2}$ orbital that explains the robustness of the neutral Mn−$(F_5Ph)_3$Cor molecule against transformation into a Mn(II) oxidation state. The configuration for the electronic S = 2 ground state is, thus, $d^1_{xz}d^1_{yz}d^1_{xy}d_{z^2}{}^1d_{x^2-y^2}{}^0$ for the 3d spin-up channel; the 3d spin-down channel remains unoccupied. The spin density of the respective orbitals is presented in Figure 2b and highlights that the dominant spin contribution is located on the metal ion. The $d_{x^2-y^2}$ orbital, which has strong overlap with the σ-orbitals of N atoms of the macrocycle, is not occupied and thus does not contribute to the total spin density (Figure 2c) of the Mn−$(F_5Ph)_3$Cor molecule.

Our results parallel the findings of Bendix et al.[23] also supporting a Mn(III), S = 2 state for the axially ligated Mn−Cor($OPPh_3$). It follows that the Mn electronic configuration in the $(F_5Ph)_3$Cor pocket is stable against the presence of the triphenylphosphine oxide ($OPPh_3$) despite the axial ligand pulling the Mn ion 0.29 Å above the macrocycle plane. Our calculations suggest the high-lying $d_{x^2-y^2}$ orbital as the origin of this robustness against ligation. For comparison, the axially ligated FeCl$(F_5Ph)_3$Cor complex has been characterized as combining Cl−Fe(III) with an $(F_5Ph)_3Cor^{2-,*}$ radical, in contrast to the Cl−Mn$(F_5Ph)_3$Cor complex, which was found to be a normal high-spin Cl−Mn(IV)$(F_5Ph)_3Cor^{3-}$ complex.

In general, the absorption L-edges are known to be more sensitive to the chemical environment of an investigated ion than the corresponding 2p XP spectra. This is related to the fact that through the X-ray absorption process core electrons are not emitted but excited into unoccupied bound or quasi-bound valence states; the involved lowest unoccupied

DOI: 10.1021/acs.jpclett.8b02525
J. Phys. Chem. Lett. 2018, 9, 6412−6420

molecular orbitals (LUMOs) are much more strongly affected by changes in the coordination geometry caused by an axial ligand, intramolecular charge transfer, or spin states. The advantage that the NEXAFS signature can act as a fingerprint for determination of the chemical state has been exploited for many molecular architectures[55] as well as tetrapyrrolic systems including MnPc[15] and MnTPP.[18] Data for Mn−corrole species, however, are missing so far. Here, we recorded high-resolution spectra of the Mn $L_{2,3}$-absorption at an undulator beamline (see also the Methods section). The measured Mn L_3-edge is depicted in Figure 3a, top panel and compared to the $L_{2,3}$-spectra calculated for the structure shown in Figure 2a. Note that the shape and positioning of components are distinct from those of other known Mn L-edges.[15,18,56−59] Thus, by simple comparison, the electronic state of the Mn in the corrole complex cannot be identified without proper theoretical treatment. Accordingly, we performed a series of calculations to investigate, e.g., the impact of spin state on the line shape of this absorption edge.

The PW supercell approach (more precisely, the XSpectra post-processing tool[60−62] of the Quantum ESPRESSO package[44]) allows straightforward investigation of surfaces and interfaces, but for calculation of XAS spectra, the core hole is included within the pseudopotential (for technical details, see the Methods section). As a consequence, screening of the electron−hole interaction by the ligands is neglected but can be covered by an empirically modified approach, where the core hole is partly taken into account.[60] In this work, we use the AE spectra calculated with the ORCA code[49] as reference to determine the optimum amount of core hole. For the $S = 2$ high-spin state, best agreement with the AE reference (blue curve in Figure 3) is obtained with about 30% core hole (orange curve). This suggests that more than 2/3 of the atomic electron−hole interaction is shielded when the Mn ion is incorporated within the corrole matrix. For the intermediate- ($S = 1$) and low-spin ($S = 0$) states, lower shielding values of 50 and 35% are deduced, respectively. This indicates that spin polarization contributes considerably to shielding of the electron−hole interaction.

For the $S = 2$ high-spin state, the Mn $L_{2,3}$-edges calculated with both methods show good agreement with the experiment, in particular, in terms of the energetic position of the main resonances A, B, C, and D (see Figure 3). However, the intensity of Peak A dominates the calculated spectrum, which is not the case in the experiment. The intensity differences and the larger broadening of the experimental spectra can be explained by intermolecular interaction between the side groups giving rise to some fluctuations in the local potentials experienced by the incorporated Mn ion. This scenario is supported by the spectrum calculated for the unit cell (see also Figure S4), which we have tentatively adapted from the free base species.[32] In reality, the molecules in the thin multilayer are expected to be more randomly oriented, and the broadening effect is expected to appear in a more pronounced way. In any case, the energetic positions of the main resonances as well as the general line shape exhibit good agreement with the experimental data and further substantiate Mn(III) in the $S = 2$ high-spin electronic ground state.

In conclusion, we performed the first X-ray spectroscopic characterization of an ultrapure metal−corrole multilayer thin film and unraveled the electronic ground state of the specific Mn center. Detailed analysis of the multiplet splitting of the Mn 3s XPS signature through DFT calculations demonstrates strong sensitivity to the formal charge as well as the spin state of the central ion and clearly indicates a Mn(III), $S = 2$ configuration. Through the simulated Mn $L_{2,3}$-edge spectra based on the AE method (ORCA), we demonstrated that the $L_{2,3}$-edge data are highly sensitive to the spin state and here strongly corroborate the high-spin ($S = 2$) electronic ground state of the Mn−$(F_5Ph)_3$Cor complex. Regarding the possible corrole radical formation, our findings line up with previous reports on other corrole complexes comprising the $(F_5Ph)_3$Cor unit[19,20,23] where no evidence of intramolecular charge transfer leading to a radical was detected. Thus, the $(F_5Ph)_3$Cor ligand expresses "*innocent*" character in the environments hitherto investigated. Comparative application of the molecular AE approach and the PW supercell approach provides the basis for studying extended systems like molecule-covered surfaces and interfaces that require periodic modeling, whereby further intriguing behavior is expected to occur.

METHODS

Sample Preparation. Manganese-5,10,15-tris(pentafluorophenyl)corrole (Mn−$(F_5Ph)_3$Cor) was synthesized according to reported procedures.[22] The quality of the employed Mn−$(F_5Ph)_3$Cor powder was analyzed by ^{1}H, ^{13}C, ^{19}F NMR (SI, Figure S5), and mass spectroscopy (SI, Figure S6), indicating above 99% purity. The thin films of Mn−$(F_5Ph)_3$Cor in the range of 10 layers were grown on a Ag(111) substrate. The Ag(111) surface of the commercial single crystal (Surface Preparation Laboratory, polished to <0.5°) was cleaned by several cycles of sputtering (Ar^+, 1 kV) and annealing (720 K) prior to deposition of the organic films. Mn−$(F_5Ph)_3$Cor was deposited by OMBE from a quartz crucible held at 483 K after prolonged degassing of the powder in vacuo at 460 K for several hours. The Ag(111) substrate was held at room temperature (300 K) during molecular deposition.

XPS and NEXAFS Spectroscopy. At the UE56/2-PGM-2 undulator beamline of the Bessy II storage ring (Berlin, Germany), a movable end station with a base pressure of 8×10^{-11} mbar and equipped with a SPECS Phoibos 100 CCD analyzer and a custom-made partial electron yield detector[63] was used. The exit slits after the monochromator were set to 10 μm, and the entrance slits after the undulator aperture were appropriately closed to reduce the photon flux and minimize beam damage caused by the very high brilliance of the photon beam. The exposure position was also systematically changed to a pristine place by moving a distance larger than the spot size between the acquisition of different spectra, in order to avoid artifacts in the XPS spectra due to radiation damage (for details, see the SI, Figure S7). The C 1s spectra were acquired with a pass energy of 10 eV, and the Mn 3s, Mn 2p, N 1s, and F 1s were acquired at a 20 eV pass energy. The photon energy was adjusted for each core-level region such that the kinetic energy of the electrons was approximately 150 eV (Mn 3s 240 eV, C 1s 435 eV, N 1s 550 eV, Mn 2p 790 eV, F 1s 850 eV). All spectra were recorded with the hemispherical analyzer in the normal emission geometry. The binding energy scale was calibrated against the Ag $3d_{5/2}$ peak (368.3 eV) or the Fermi edge (0 eV) of the Ag(111) substrate. The experimental spectra were fitted with a variable number of spectral components exhibiting a Voigt line shape after a Shirley (C 1s), linear (F 1s), or polynomial background of fifth order (N 1s) was subtracted from the raw data.

On the same beamline, NEXAFS spectra were recorded in the partial electron yield mode with a monochromator grating

DOI: 10.1021/acs.jpclett.8b02525
J. Phys. Chem. Lett. 2018, 9, 6412−6420

of 1200 l/ and exit slit widths of 60 μm. A retarding voltage of −450 V was used at the Mn L-edge. The spectra were measured at different incident angles θ (7° and 90°) between the E-vector of the incident light (90% linear polarization[64]) and the surface normal. To improve the signal-to-noise ratio, several spectra were collected at previously unexposed places, and the average is presented in this work. After subtraction of the signal of the bare crystal from the raw data, the measured spectra were normalized to an edge jump of one.

DFT for the Molecular Systems. 1. Plane-Wave (PW) Pseudopotential Approach. The PW DFT calculations were performed with the Quantum ESPRESSO package.[44] The PBE functional[45] and the PBE+*U* extension (with self-consistently determined U = 4.007 eV)[46] were used to model correlation and exchange interactions complemented with dispersion correction (DFT-D).[65] For the description of the electron−ion interaction, we applied ultrasoft pseudopotentials of the projector-augmented wave (PAW) type.[66] A kinetic cutoff energy of 75 Ry was used for the PW basis set. Structure relaxation was performed for Mn−corrole in the solid state (two molecules in the unit cell, cf. Figure S4) and for isolated molecules (in periodically repeated supercells, large boxes of 30 × 30 × 24 Å^3 size, in order to minimize intermolecular interactions). Structural optimization of the investigated systems was performed with convergence criteria of 0.03 eV/nm for forces and 10^{-6} eV for total energy.

X-ray absorption (NEXAFS/XANES) Mn $L_{2,3}$-edges spectra (for PBE-relaxed structures) were calculated with the XSpectra code[60−62] of the Quantum ESPRESSO package. For all calculations, we used ultrasoft PAW pseudopotentials with a respective occupation of the Mn 2p shell. Full core hole as well as half core hole (50%) and no core hole (0%) approximations (and also some core hole values in between; see Figures S2 and S3) were tested with respect to their influence on the calculated Mn L_3-edge. Respective pseudopotentials were generated with the Troullier−Martins[67] pseudization scheme. In the NEXAFS calculation, we used, if not otherwise stated, a 1 × 1 × 1 *k*-point grid (Γ-point approximation). The onset of the calculated excitation energies was aligned with experiment using the L_3-edge. Finally, the estimated spectra were broadened by convolution with a Lorentzian function (half-width at half-maximum set to 0.2 eV). Further details of the method and its application onto free base corroles can be found elsewhere.[32,33]

2. All-Electron (AE) Calculations. To calculate the Mn L-edge spectra, we also used the restricted open-shell configuration interaction with single excitations (ROCIS) approach based on molecular DFT (DFT/ROCIS)[48] with spin−orbit coupling (SOC) being incorporated by a molecular Russell−Saunders scheme.[68] The AE calculations utilized the hybrid Becke3−Lee−Yang−Parr (B3LYP) XC functional[50−52] and def2-TZVP(-f) basis set[69] and have been performed with the ORCA suite of programs.[49] The X-ray absorption spectra with respect to the L_3-edge energy were subsequently obtained from DFT/ROCIS calculated intensities and transition energies by imposing again a Lorentzian broadening of 0.2 eV.

■ ASSOCIATED CONTENT

Supporting Information

The Supporting Information is available free of charge on the ACS Publications website at DOI: 10.1021/acs.jpclett.8b02525.

Relativistic spin−orbit splitting values of the Mn 2p core level, PDOS plots of Mn 3d orbitals and their energies, PBE-calculated Mn L-edge spectra for the different spin states and for various amounts of effective core holes, (tentative) model for the molecular crystal, further information on beam damage and sample purity, and related references (PDF)

■ AUTHOR INFORMATION

Corresponding Authors

*E-mail: florian.klappenberger@tum.de (F.K.).
*E-mail: uwe.gerstmann@upb.de (U.G.).

ORCID

Francesco Allegretti: 0000-0001-6141-7166
Wolfgang Schöfberger: 0000-0002-8055-8906
Johannes V. Barth: 0000-0002-6270-2150
Florian Klappenberger: 0000-0002-2877-6105

Notes

The authors declare no competing financial interest.

■ ACKNOWLEDGMENTS

We thank Peter Feulner, Peter S. Deimel, and David A. Duncan for mounting and setting up the end station at the Bessy II storage ring. This work was made possible via the Austrian Science Fund (FWF) project D-A-CH i958. Funding provided by the European Union via ERC Advanced Grant MolArt (Grant 247299), the German Research Foundation (DFG) via KL 2294/3-1, SPP 1601, and TRR 142, the Munich-Centre for Advanced Photonics (MAP), and the Austrian Science Fund (FWF-P28167) is also gratefully acknowledged. Computational resources were allocated at the Paderborn Center for Parallel Computing (PC^2). We also thank the Helmholtz-Zentrum Berlin (HZB) for financial support and for the allocation of synchrotron radiation beam time.

■ REFERENCES

(1) Kadish, K. M.; Schmith, K. M.; Guilard, R. *The Porphyrin Handbook, Applications: Past, Present and Future*; Academic Press: San Diego, CA, 2000.
(2) Gottfried, J. M. Surface Chemistry of Porphyrins and Phthalocyanines. *Surf. Sci. Rep.* **2015**, *70*, 259−379.
(3) Auwärter, W.; Écija, D.; Klappenberger, F.; Barth, J. V. Porphyrins at Interfaces. *Nat. Chem.* **2015**, *7*, 105−120.
(4) Aviv-Harel, I.; Gross, Z. Aura of Corroles. *Chem. - Eur. J.* **2009**, *15*, 8382−8394.
(5) Gross, Z. High-Valent Corrole Metal Complexes. *JBIC, J. Biol. Inorg. Chem.* **2001**, *6*, 733−738.
(6) Aviv, I.; Gross, Z. Corrole-Based Applications. *Chem. Commun.* **2007**, 1987−1999.
(7) Kulkarni, A. A.; Daugulis, O. Direct Conversion of Carbon-Hydrogen into Carbon-Carbon Bonds by First-Row Transition-Metal Catalysis. *Synthesis* **2009**, 4087−4109.
(8) Royer, S.; Duprez, D. Catalytic Oxidation of Carbon Monoxide over Transition Metal Oxides. *ChemCatChem* **2011**, *3*, 24−65.
(9) Batten, S. R.; Murray, K. S. Structure and Magnetism of Coordination Polymers Containing Dicyanamide and Tricyanomethanide. *Coord. Chem. Rev.* **2003**, *246*, 103−130.
(10) Aromi, G.; Brechin, E. K., Synthesis of 3d Metallic Single-Molecule Magnets. In *Structure and Bonding*; 2006; Vol. *122*, pp 1−67.
(11) Li, J. R.; Sculley, J.; Zhou, H. C. Metal-Organic Frameworks for Separations. *Chem. Rev.* **2012**, *112*, 869−932.

DOI: 10.1021/acs.jpclett.8b02525
J. Phys. Chem. Lett. 2018, 9, 6412−6420

(12) Yoon, M.; Srirambalaji, R.; Kim, K. Homochiral Metal-Organic Frameworks for Asymmetric Heterogeneous Catalysis. *Chem. Rev.* **2012**, *112*, 1196−1231.
(13) Zacher, D.; Shekhah, O.; Wöll, C.; Fischer, R. A. Thin Films of Metal-Organic Frameworks. *Chem. Soc. Rev.* **2009**, *38*, 1418−1429.
(14) Beggan, J. P.; Krasnikov, S. A.; Sergeeva, N. N.; Senge, M. O.; Cafolla, A. A. Control of the Axial Coordination of a Surface-Confined Manganese(III) Porphyrin Complex. *Nanotechnology* **2012**, *23*, 235606.
(15) Petraki, F.; Peisert, H.; Hoffmann, P.; Uihlein, J.; Knupfer, M.; Chassé, T. Modification of the 3d-Electronic Configuration of Manganese Phthalocyanine at the Interface to Gold. *J. Phys. Chem. C* **2012**, *116*, 5121−5127.
(16) den Boer, D.; Li, M.; Habets, T.; Iavicoli, P.; Rowan, A. E.; Nolte, R. J. M.; Speller, S.; Amabilino, D. B.; De Feyter, S.; Elemans, J. A. A. W. Detection of Different Oxidation States of Individual Manganese Porphyrins During their Reaction with Oxygen at a Solid/Liquid Interface. *Nat. Chem.* **2013**, *5*, 621−627.
(17) Grumelli, D.; Wurster, B.; Stepanow, S.; Kern, K. Bio-Inspired Nanocatalysts for the Oxygen Reduction Reaction. *Nat. Commun.* **2013**, *4*, 2904.
(18) Murphy, B. E.; Krasnikov, S. A.; Sergeeva, N. N.; Cafolla, A. A.; Preobrajenski, A. B.; Chaika, A. N.; Lübben, O.; Shvets, I. V. Homolytic Cleavage of Molecular Oxygen by Manganese Porphyrins Supported on Ag(111). *ACS Nano* **2014**, *8*, 5190−5198.
(19) Gross, Z.; Golubkov, G.; Simkhovich, L. Epoxidation Catalysis by a Manganese Corrole and Isolation of an Oxomanganese(V) Corrole. *Angew. Chem., Int. Ed.* **2000**, *39*, 4045−4047.
(20) Golubkov, G.; Bendix, J.; Gray, H. B.; Mahammed, A.; Goldberg, I.; DiBilio, A. J.; Gross, Z. High-Valent Manganese Corroles and the First Perhalogenated Metallocorrole Catalyst. *Angew. Chem., Int. Ed.* **2001**, *40*, 2132−2134.
(21) Liu, H. Y.; Mahmood, M. H. R.; Qiu, S. X.; Chang, C. K. Recent Developments in Manganese Corrole Chemistry. *Coord. Chem. Rev.* **2013**, *257*, 1306−1333.
(22) Schöfberger, W.; Faschinger, F.; Chattopadhyay, S.; Bhakta, S.; Mondal, B.; Elemans, J. A. A. W.; Müllegger, S.; Tebi, S.; Koch, R.; Klappenberger, F.; et al. A Bifunctional Electrocatalyst for Oxygen Evolution and Oxygen Reduction Reactions in Water. *Angew. Chem., Int. Ed.* **2016**, *55*, 2350−2355.
(23) Bendix, J.; Gray, H. B.; Golubkov, G.; Gross, Z. High-Field (High-Frequency) EPR Spectroscopy and Structural Characterization of a Novel Manganese(III) Corrole. *Chem. Commun.* **2000**, 1957−1958.
(24) Krzystek, J.; Telser, J.; Hoffman, B. M.; Brunel, L. C.; Licoccia, S. High-Frequency and Field EPR Investigation of (8,12-diethyl-2,3,7,13,17,18-Hexamethylcorrolato)manganese(III). *J. Am. Chem. Soc.* **2001**, *123*, 7890−7897.
(25) Will, S.; Lex, J.; Vogel, E.; Schmickler, H.; Gisselbrecht, J. P.; Haubtmann, C.; Bernard, M.; Gorss, M. Nickel and Copper Corroles: Well-Known Complexes in a New Light. *Angew. Chem., Int. Ed. Engl.* **1997**, *36*, 357−361.
(26) Schweyen, P.; Brandhorst, K.; Wicht, R.; Wolfram, B.; Bröring, M. The Corrole Radical. *Angew. Chem., Int. Ed.* **2015**, *54*, 8213−8216.
(27) Ghosh, A.; Wondimagegn, T.; Parusel, A. B. J. Electronic Structure of Gallium, Copper, and Nickel Complexes of Corrole. High-Valent Transition Metal Centers versus Noninnocent Ligands. *J. Am. Chem. Soc.* **2000**, *122*, 5100−5104.
(28) Tebi, S.; Paszkiewicz, M.; Aldahhak, H.; Allegretti, F.; Gonglach, S.; Haas, M.; Waser, M.; Deimel, P. S.; Aguilar, P. C.; Zhang, Y.-Q.; et al. On-Surface Site-Selective Cyclization of Corrole Radicals. *ACS Nano* **2017**, *11*, 3383−3391.
(29) Goldberg, D. P.; Telser, J.; Krzystek, J.; Montalban, A. G.; Brunel, L. C.; Barrett, A. G. M.; Hoffman, B. M. EPR Spectra from "EPR-Silent" Species: High-Field EPR Spectroscopy of Manganese-(III) Porphyrins. *J. Am. Chem. Soc.* **1997**, *119*, 8722−8723.
(30) Gross, Z.; Barzilay, C. M. Halogen to Metal π-Donation in Metalloporphyrins. *Chem. Commun.* **1998**, 1105−1107.
(31) Turner, P.; Gunter, M. J. C-13 NMR-Spectroscopy, Electron Spin Distributions, and Valence State of Pentacoordinate Manganese Tetraphenylporphyrin Complexes. *Inorg. Chem.* **1994**, *33*, 1406−1415.
(32) Aldahhak, H.; Paszkiewicz, M.; Allegretti, F.; Duncan, D. A.; Tebi, S.; Deimel, P. S.; Casado Aguilar, P.; Zhang, Y. Q.; Papageorgiou, A. C.; Koch, R.; et al. X-ray Spectroscopy of Thin Film Free-Base Corroles: A Combined Theoretical and Experimental Characterization. *J. Phys. Chem. C* **2017**, *121*, 2192−2200.
(33) Aldahhak, H.; Paszkiewicz, M.; Rauls, E.; Allegretti, F.; Tebi, S.; Papageorgiou, A. C.; Zhang, Y. Q.; Zhang, L.; Lin, T.; Paintner, T.; et al. Identifying On-Surface Site-Selective Chemical Conversions by Theory-Aided NEXAFS Spectroscopy: The Case of Free-Base Corroles on Ag(111). *Chem. - Eur. J.* **2018**, *24*, 6787−6797.
(34) Marbach, H. Surface-Mediated in Situ Metalation of Porphyrins at the Solid−Vacuum Interface. *Acc. Chem. Res.* **2015**, *48*, 2649−2658.
(35) Huang, H. C.; Wang, C. H.; Shown, I.; Chang, S. T.; Hsu, H. C.; Du, H. Y.; Chen, L. C.; Chen, K. H. High-Performance Pyrolyzed Iron Corrole as a Potential Non-Precious Metal Catalyst for PEMFCs. *J. Mater. Chem. A* **2013**, *1*, 14692−14699.
(36) Uihlein, J.; Peisert, H.; Adler, H.; Glaser, M.; Polek, M.; Ovsyannikov, R.; Bauer, M.; Chasse, T. Strong Interaction of MnPc on Ni(111): Influence of Graphene Buffer Layer. *J. Phys. Chem. C* **2014**, *118*, 28671−28678.
(37) Gupta, R. P.; Sen, S. K. Calculation of Multiplet Structure of Core *p*-Vacancy Levels. *Phys. Rev. B* **1974**, *10*, 71−77.
(38) Gupta, R. P.; Sen, S. K. Calculation of Multiplet Structure of Core *p*-Vacancy Levels. II. *Phys. Rev. B* **1975**, *12*, 15−19.
(39) Nesbitt, H. W.; Banerjee, D. Interpretation of XPS Mn(2p) Spectra of Mn Oxyhydroxides and Constraints on the Mechanism of MnO_2 Precipitation. *Am. Mineral.* **1998**, *83*, 305−315.
(40) Buitendach, E. B.; Erasmus, E.; Niemantsverdriet, W. J.; Swarts, C. J. Properties of Manganese(III) Ferrocenyl-β-Diketonato Complexes Revealed by Charge Transfer and Multiplet Splitting in the Mn 2p and Fe 2p X-Ray Photoelectron Envelopes. *Molecules* **2016**, *21*, 1427−1441.
(41) Cerrato, J. M.; Hochella, M. F.; Knocke, W. R.; Dietrich, A. M.; Cromer, T. F. Use of XPS to Identify the Oxidation State of Mn in Solid Surfaces of Filtration Media Oxide Samples from Drinking Water Treatment Plants. *Environ. Sci. Technol.* **2010**, *44*, 5881−5886.
(42) Galakhov, V. R.; Demeter, M.; Bartkowski, S.; Neumann, M.; Ovechkina, N. A.; Kurmaev, E. Z.; Lobachevskaya, N. I.; Mukovskii, Y. M.; Mitchell, J.; Ederer, D. L. Mn 3s Exchange Splitting in Mixed-Valence Manganites. *Phys. Rev. B: Condens. Matter Mater. Phys.* **2002**, *65*, 113102.
(43) Fujiwara, M.; Matsushita, T.; Ikeda, S. Evaluation of Mn3s X-Ray Photoelectron Spectroscopy for Characterization of Manganese Complexes. *J. Electron Spectrosc. Relat. Phenom.* **1995**, *74*, 201−206.
(44) Giannozzi, P.; Baroni, S.; Bonini, N.; Calandra, M.; Car, R.; Cavazzoni, C.; Ceresoli, D.; Chiarotti, G. L.; Cococcioni, M.; Dabo, I.; et al. QUANTUM ESPRESSO: a Modular and Open-Source Software Project for Quantum Simulations of Materials. *J. Phys.: Condens. Matter* **2009**, *21*, 395502.
(45) Perdew, J. P.; Burke, K.; Ernzerhof, M. Generalized Gradient Approximation Made Simple. *Phys. Rev. Lett.* **1996**, *77*, 3865−3868.
(46) Cococcioni, M.; de Gironcoli, S. Linear Response Approach to the Calculation of the Effective Interaction Parameters in the LDA+U Method. *Phys. Rev. B: Condens. Matter Mater. Phys.* **2005**, *71*, 035105.
(47) Kulik, H. J.; Cococcioni, M.; Scherlis, D. A.; Marzari, N. Density Functional Theory in Transition-Metal Chemistry: A Self-Consistent Hubbard U Approach. *Phys. Rev. Lett.* **2006**, *97*, 103001.
(48) Roemelt, M.; Neese, F. Excited States of Large Open-Shell Molecules: An Efficient, General, and Spin-Adapted Approach Based on a Restricted Open-Shell Ground State Wave function. *J. Phys. Chem. A* **2013**, *117*, 3069−3083.
(49) Neese, F. Software Update: the ORCA Program System, version 4.0. *Wiley Interdiscip. Rev.-Comput. Mol. Sci.* **2018**, *8*, e1327.

DOI: 10.1021/acs.jpclett.8b02525
J. Phys. Chem. Lett. 2018, 9, 6412−6420

(50) Becke, A. D. Density-Functional Exchange-Energy Approximation with Correct Asymptotic-Behavior. *Phys. Rev. A: At., Mol., Opt. Phys.* **1988**, *38*, 3098−3100.
(51) Becke, A. D. Density-Functional Thermochemistry. 3. The Role of Exact Exchange. *J. Chem. Phys.* **1993**, *98*, 5648−5652.
(52) Lee, C. T.; Yang, W. T.; Parr, R. G. Development of the Colle-Salvetti Correlation-Energy Formula into a Functional of the Electron-Density. *Phys. Rev. B: Condens. Matter Mater. Phys.* **1988**, *37*, 785−789.
(53) Ghosh, A. Electronic Structure of Corrole Derivatives: Insights from Molecular Structures, Spectroscopy, Electrochemistry, and Quantum Chemical Calculations. *Chem. Rev.* **2017**, *117*, 3798−3881.
(54) Licoccia, S.; Morgante, E.; Paolesse, R.; Polizio, F.; Senge, M. O.; Tondello, E.; Boschi, T. Tetracoordinated Manganese(III) Alkylcorrolates. Spectroscopic Studies and the Crystal and Molecular Structure of (7,13-dimethyl-2,3,8,12,17,18-hexaethylcorrolato)-manganese(III). *Inorg. Chem.* **1997**, *36*, 1564−1570.
(55) Klappenberger, F. Two-Dimensional Functional Molecular Nanoarchitectures - Complementary Investigations with Scanning Tunneling Microscopy and X-Ray Spectroscopy. *Prog. Surf. Sci.* **2014**, *89*, 1−55.
(56) Cramer, S. P.; DeGroot, F. M. F.; Ma, Y.; Chen, C. T.; Sette, F.; Kipke, C. A.; Eichhorn, D. M.; Chan, M. K.; Armstrong, W. H.; Libby, E.; et al. Ligand-Field Strengths and Oxidation-States from Manganese L-Edge Spectroscopy. *J. Am. Chem. Soc.* **1991**, *113*, 7937−7940.
(57) Gilbert, B.; Frazer, B. H.; Belz, A.; Conrad, P. G.; Nealson, K. H.; Haskel, D.; Lang, J. C.; Srajer, G.; De Stasio, G. Multiple Scattering Calculations of Bonding and X-Ray Absorption Spectroscopy of Manganese oxides. *J. Phys. Chem. A* **2003**, *107*, 2839−2847.
(58) Allegretti, F.; Franchini, C.; Bayer, V.; Leitner, M.; Parteder, G.; Xu, B.; Fleming, A.; Ramsey, M. G.; Podloucky, R.; Surnev, S.; et al. Epitaxial Stabilization of MnO(111) Overlayers on a Pd(100) Surface. *Phys. Rev. B: Condens. Matter Mater. Phys.* **2007**, *75*, 224120.
(59) Bayer, V.; Podloucky, R.; Franchini, C.; et al. Formation of Mn_3O_4(001) on MnO(001): Surface and Interface Structural Stability. *Phys. Rev. B: Condens. Matter Mater. Phys.* **2007**, *76*, 165428.
(60) Bunau, O.; Calandra, M. Projector Augmented Wave Calculation of X-Ray Absorption Spectra at the $L_{2,3}$ Edges. *Phys. Rev. B: Condens. Matter Mater. Phys.* **2013**, *87*, 205105.
(61) Gougoussis, C.; Calandra, M.; Seitsonen, A. P.; Mauri, F. First-Principles Calculations of X-Ray Absorption in a Scheme Based on Ultrasoft Pseudopotentials: From α-Quartz to High-T_c Compounds. *Phys. Rev. B: Condens. Matter Mater. Phys.* **2009**, *80*, 075102.
(62) Taillefumier, M.; Cabaret, D.; Flank, A. M.; Mauri, F. X-Ray Absorption Near-Edge Structure Calculations with the Pseudopotentials: Application to the K Edge in Diamond and α-Quartz. *Phys. Rev. B: Condens. Matter Mater. Phys.* **2002**, *66*, 195107.
(63) Blobner, F.; Neppl, S.; Feulner, P. A Versatile Partial Electron Yield Detector with Large Acceptance Angle and Well-Defined Threshold Energy and Gain. *J. Electron Spectrosc. Relat. Phenom.* **2011**, *184*, 483−486.
(64) Duncan, D. A.; Unterberger, W.; Kreikemeyer-Lorenzo, D.; Woodruff, D. P. Uracil on Cu(110): A Quantitative Structure Determination by Energy-Scanned Photoelectron Diffraction. *J. Chem. Phys.* **2011**, *135*, 014704.
(65) Ortmann, F.; Bechstedt, F.; Schmidt, W. G. Semiempirical van der Waals Correction to the Density Functional Description of Solids and Molecular Structures. *Phys. Rev. B: Condens. Matter Mater. Phys.* **2006**, *73*, 205101.
(66) Blöchl, P. E. Projector Augmented-Wave Method. *Phys. Rev. B: Condens. Matter Mater. Phys.* **1994**, *50*, 17953−17979.
(67) Troullier, N.; Martins, J. L. Efficient Pseudopotentials for Plane-Wave Calculations. *Phys. Rev. B: Condens. Matter Mater. Phys.* **1991**, *43*, 1993−2006.
(68) Roemelt, M.; Maganas, D.; DeBeer, S.; Neese, F. A Combined DFT and Restricted Open-Shell Configuration Interaction Method Including Spin-Orbit Coupling: Application to Transition Metal L-Edge X-Eay Absorption Spectroscopy. *J. Chem. Phys.* **2013**, *138*, 204101.
(69) Weigend, F.; Ahlrichs, R. Balanced Basis Sets of Split Valence, Triple Zeta Valence and Quadruple Zeta Valence Quality for H to Rn: Design and Assessment of Accuracy. *Phys. Chem. Chem. Phys.* **2005**, *7*, 3297−3305.

DOI: 10.1021/acs.jpclett.8b02525
J. Phys. Chem. Lett. 2018, 9, 6412−6420